Prediction of pulsed-laser powder deposits' shape profiles using a back-propagation artificial neural network

M M Mahapatra* and **L Li**
Department of Mechanical and Aerospace Engineering, Utah State University, Logan, Utah, USA

The manuscript was received on 16 May 2008 and was accepted after revision for publication on 28 August 2008.

DOI: 10.1243/09544054JEM1228

Abstract: The cross-sectional shape profile geometry of blown powder clad deposit is important for overall structural integrity of the clad layer. The penetration zone of the clad deposit is represented within its shape profile geometry. The shape profile geometry of the clad deposit is also important for thermomechanical modelling. Although a rough estimation of blown powder clad deposit shape profile can be made based on the powder feeding parameters using empirical formulae, it may not be sufficiently accurate to be used in a thermomechanical model, as it may lead to inaccuracy in the prediction of temperature distributions, residual stresses, and distortion. The pulsed-laser blown powder deposition process is a highly coupled multivariable problem. Hence the deterministic numerical-methods-based prediction of pulsed-laser powder deposit shape profile geometry is time consuming, costly, and may not be adequate to predict the profile geometry over a wide range of varying process parameters. The present investigation deals with the cross-sectional shape profile geometry modelling of the pulsed-laser assisted superalloy powder deposition (PLPD) process using a soft computing approach. A simple yet effective mapping technique was used in the present work to map the experimentally obtained shape profiles of the powder deposits. The mapped characteristics of the powder deposits' shape profiles were used in the back-propagation artificial neural network (ANN) modelling of the PLPD process. The present modelling technique can be conveniently used to incorporate the PLPD shape profile geometry parameters in thermomechanical analyses for accurate prediction of temperature distributions and residual stresses. Based on the present soft computing modelling methodology, an estimation of top reinforcement and penetration zone shape boundaries of a blown powder clad deposit can also be made.

Keywords: Nd–Yag laser, pulsed-laser superalloy powder depositions (PLPD), soft computing, artificial neural network (ANN), back-propagation network (BPN), deposition shape profiles

1 INTRODUCTION

Molten metal deposition processes such as welding and cladding are substantially non-linear and highly coupled multivariable systems [**1**–**3**]. Frequently, not all variables affecting the quality of welding and cladding depositions are known or easily quantifiable. Thus many investigators have resorted to prediction of welding and cladding deposit characteristics based on experimental results using soft computing techniques such as artificial neural networks (ANNs) [**1**–**3**].

The requirement in the present investigation was realized during the thermomechanical numerical modelling of the superalloy repairing process using pulsed-laser powder depositions (PLPDs) to predict thermophysical effects such as temperature distributions and residual stresses in the clad layers. For numerical modelling of the PLPD process, precise incorporation of the clad deposit shape profile in the model was required. Efforts were made to estimate the shape profile geometry of the PLPD deposits from the empirical formulae considering powder-feeding

**Corresponding author: Department of Mechanical and Aerospace Engineering, Utah State University, Logan 84341, Utah, USA. email: man.patra@engineering.usu.edu; manasmohan2@gmail.com; leijun.li@usu.edu*

parameters. However, the estimated deposit shape profiles from the empirical formulae were not sufficiently accurate. As the blown powder deposition process is highly coupled and multivariable, time-consuming numerical modelling of the PLPD shape profile geometry was not carried out. Instead a database of the mapped characteristics of the deposits' shape profiles was obtained based on a design matrix for the PLPD experiments. These mapped characteristics of the deposit profiles were used for training a back-propagation ANN. The trained ANN model was further used to predict the deposit shape profiles.

Kim *et al.* were among the first few investigators to predict the entire weld bead shape geometry profile using the ANN based soft computing approach [**4**]. The mapping methodology of the weld bead was not described in detail in their work [**4**]. Both regression analysis and the ANN technique were used by Kim *et al*. to model the weld bead shape profiles, and the suitability of ANN over the regression analysis was reported in their work [**4**]. A back-propagation ANN model was used by Kanti and Rao for the prediction of bead profile geometry of pulsed gas metal arc (GMA) welds [**5**]. In their ANN model the weld top reinforcement and the penetration zone were assumed to be convex and concave in shape respectively [**5**]. However, during the present investigation it was observed that the penetration zone of the PLPD deposits might not always represent an exact concave shape.

The PLPD-clad profiles are important characteristics of the superalloy component repairing process. The clad deposition height, penetrations, and the overall profile are dependent on the input process parameters [**6**]. Stresses in the substrate, deformations of the substrate, and even the stray grain formation in cladding are dependent on the nature of reinforcement of the deposition (i.e. deposition shape profiles) [**6**, **7**]. Formations of stray grains in superalloy cladding are believed to be process related [**7**]. Not many investigators have predicted the superalloy clad geometry shape profile of the PLPD process using soft computing approaches.

The shape profiles of laser-clad tracks were successfully predicted by Liu and Li using an analytical approach [**8**]. The clad track heights at different positions were considered in their analytical model for prediction of the final clad shape profile [**8**]. The cladding heights of the laser solid freeform fabrication process were predicted by Toyserkani and Alimardani using a neuro-fuzzy approach [**9**]. It was reported in their work that the laser solid freeform fabrication process was highly non-linear and could not be modelled analytically [**9**]. The PLPD process is also highly non-linear and it is difficult to model its shape profiles using analytical approaches. For the better training of the network more than one hidden layer were utilized by Toyserkani and Alimardani in the ANN model of the laser solid freeform fabrication process [**9**]. The weld pool shape was also modelled by Vitek *et al.* using an ANN and the suitability of the soft computing approach was reported [**10**]. The laser cladding track angles were predicted by Onwubolu *et al.* by using the response surface methodology [**11**]. The complete shape profile geometries of the deposits were not mentioned in their work [**11**].

Works related to the prediction of shape profiles of pulsed-laser powder depositions are rarely found in the literature. Often it is observed from the literature that the soft computing based prediction of clad characteristics is limited to deposit height, deposit width, and depth of penetration, from which the exact graphical representation of the deposit shape profile geometry might not be possible [**9–14**]. For example, the heights of two clad deposits might be similar, but differences may exist with regard to their reinforcement profiles. Hence the complete mapping of the PLPD profile geometry is required for precise graphical representation. In the present investigation the detailed shape profile geometry of the PLPD has been predicted rather than the characteristic dimensions. It is also observed that an ANN can be trained to predict the detailed shape profiles of the PLPD deposits from a set of experimental data.

1.1 Back-propagation ANN modelling of PLPD shape profiles

Artificial neural networks are parallel computational models comprising densely adaptive units; they have become popular among researchers of non-linear problems such as welding and cladding. A very important feature of these networks is their adaptive nature, where they learn from the relationship patterns of input and output. This feature makes such computational models very appealing in application domains such as welding/cladding problems, where the researcher has an incomplete understanding of the problems to be solved but where training data are readily available [**1–3**]. The neural networks are useful in solving non-linear problems because of their high execution speed and adaptive learning capability related to data during the training [**1–3**]. To capture the essence of a biological neuron system the artificial neuron in an ANN receives a number of inputs either from original data or from other neurons in the network. Each input is routed through a connection and the input signal strength is designated as 'weight'. These weights correspond to the synaptic efficiency of a biological neuron. The weighted sum of the inputs is formed and the threshold is subtracted to compose the activation of the neuron. The activation signal is passed through an activation function also known as a transfer function [**1–3**].

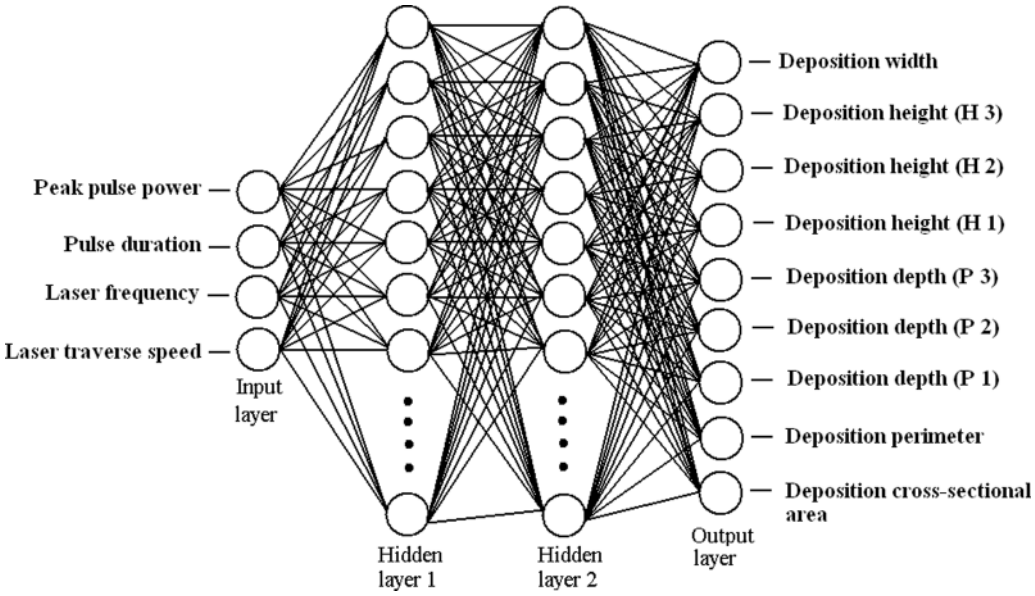

Fig. 1 ANN model used for predicting PLPD shape profiles

In this work, back-propagating (BPN) algorithm based neural networks architecture was used. The most widely used example of a neural network training algorithm is back propagation. Many investigators have successfully used the back-propagation ANN modelling technique for weldment characteristics modelling [**1**–**3**, **13**–**14**]. Some investigators have also used the back-propagation neural network for weld bead geometry profile prediction [**4**–**5**].

In back propagation the gradient vector of the error surface is calculated. This vector points in the direction of the steepest descent from the current point, indicating that moving along it for a short distance will decrease the error. A sequence of such moves will eventually find a minimum of some kind. Large steps may converge too quickly, but may also overstep the solutions. Small steps may go in the correct direction but require a large number of iterations. This is represented as a constant, known as the learning rate. The correct learning rate is application dependent. A processing element accepts one or more signals, which may be produced by other processing elements or applied externally (e.g. provided by a process sensor). The various signals are individually amplified, or weighted, and then summed together within the processing element. The transfer function used in the back-propagation network, known as sigmoid transfer function, is [**1**–**3**]

$$f(s) = \frac{1}{1 + e^{-s}} \tag{1}$$

where s is the sum of the node inputs. It should be noted that the node output will be confined to the range $0 < f(s) < 1$. The ANN progresses iteratively through a number of epochs. For each epoch, the training cases are in turn submitted to the network and actual output and the targets are compared and errors are calculated. This error together with the error surface gradients is used to adjust the weights. This process is repeated until a satisfactory level of training is achieved. The training stops when the error reaches an acceptable level. A back-propagation network used in the present investigation is shown in Fig. 1. Neurons are arranged in a distinct layered topology. The input units simply serve to introduce the values of the input variables. The input variables for problems are decided according to the specificity of the problem.

2 EXPERIMENTAL DETAILS OF THE PLPD PROCESS

During the experiments single PLPD tracks of René 80 powders were made on GTD 111 turbine engine material. The experimental set-up for the PLPD process is shown in Fig. 2. A HAAS™ HL54P pulsed wave laser was used for the experiments involving the deposition of superalloys [**15**]. The HAAS HL54P is a square wave pulsing neodymium-doped yttrium aluminium garnet (Nd:YAG) laser with arrangements to deliver the power through fibre optical cables to the workpiece. The average maximum power output of the HAAS HL54P pulse laser is 50 W. Maximum peak pulse power of this laser is 5 kW. A Bay State Surface Technologies model 1200 powder feeder was used to inject the powder into the clad pool [**16**].

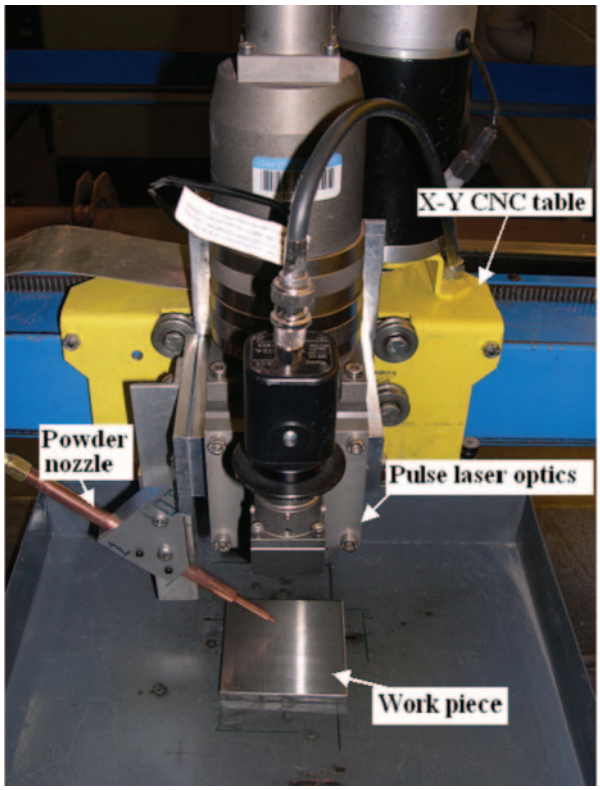

Fig. 2 Pulsed-laser powder deposition set-up

The powder injection nozzle used in the experiment was manufactured in-house and had a circular opening of 1.5 mm diameter, positioned 15 mm away from the clad melt pool. The powder was injected into the leading edge of the melt pool. The substrate material was ground with an eighty-grit grind wheel to remove the oxide layer. Acetone was also used to clean the surface of the substrate material before the deposition.

The repair work required deposition to be carried out top down with respect to the crystal growth direction. René 80 is the closest matching filler material to GTD 111 that is commercially available. The René 80 powder size used was 125–325 μm. The compositions of GTD 111 and the René 80 alloys are given in Table 1.

For the experiment the powder output (or r/min) was held constant at 4 r/min. The equivalent flowrate was 30 g/min. The pressure of the argon that carried the powder to the melt pool was held constant at 25 psi. The angle of the nozzle was held constant at 45°. The powder was injected into the melt pool directly, but from a trailing powder nozzle instead of a leading nozzle for the depositions. Process efficiency requires the spot size of the laser to be large to improve the percentage of the powder being injected into the melt pool. In these experiments the spot size was 1 mm in diameter.

Table 1 Alloying compositions of GTD 111 and René 80 [7]

Element	GTD 111	PARXAIR Ni138 (René 80)
Al	2.8–3.2	2.80
B	0.01–0.02	0.01
C	0.08–0.12	0.18
Co	9.0–10.0	9.66
Cr	13.7–14.3	14.09
Cu	–	0.05
Fe	–	0.05
Hf	0.02–0.08	0.10
Mg	–	0.001
Mn	–	0.10
Mo	1.3–1.7	4.03
N	–	0.0049
Nb	–	0.05
O	–	0.01
P	–	0.005
S	–	0.0017
Se	–	0.005
Si	–	0.10
Ta	2.5–3.1	0.10
Ti	4.8–5.1	4.83
V	–	0.05
W	3.5–4.1	3.91
Zr	0.02–0.08	0.06
Ni	Balance	Balance

The power and duration of the pulsing were directly set in the laser power source. High, medium, and low levels were selected for power and duration based on earlier experiments on the GTD 111 alloy (Table 2). The third parameter that was changed was the spacing between each pulse. This was determined by adjusting the frequency and the travel speed until the desired spacing was reached. Certain levels in the experiments exceeded the power limit of the machine, so the frequency and travel speed parameters were decreased to compensate. A detailed list of the process parameters selected and experimented for 27 samples can be seen in Table 2. A single track and layers of superalloy PLPD obtained during the investigation are shown in Fig. 3.

2.1 Graphical mapping of the PLPD shape profile

A schematic diagram of the macrostructure zones of a single-track powder deposition is presented in Fig. 4. The deposition width designated as BW is indicated by the line A–G and is divided into six equal segments as A–B, B–C, C–D, D–E, E–F, and F–G. The connecting lines (A–B. . .L–A) describe the top reinforcements. Considering the heights of top reinforcements at these segments (H1, H2, and H3, see Fig. 4), the top reinforcement can be graphically represented bounded by the lines A–B. . .L–A.

Similarly, if the depths of penetration (P1, P2, and P3, see Fig. 4) at the line segments A–B, B–C, C–D, D–E, E–F, and F–G are known, then the area

Table 2 PLPD parameters used for training the ANN

	Low		Medium		High	
Pulse power (kW)	2.5		3.0		3.5	
Pulse duration (ms)	1.5		2.0		2.5	
Spot spacing (mm)	0.2		0.15		0.1	
	Laser frequency (Hz)	Laser traverse speed (mm/s)	Laser frequency (Hz)	Laser traverse speed (mm/s)	Laser frequency (Hz)	Laser traverse speed (mm/s)
	5.0	1.27	8.0	1.27	8.0	0.804
	2.5	0.635	4.0	0.635	4.0	0.381

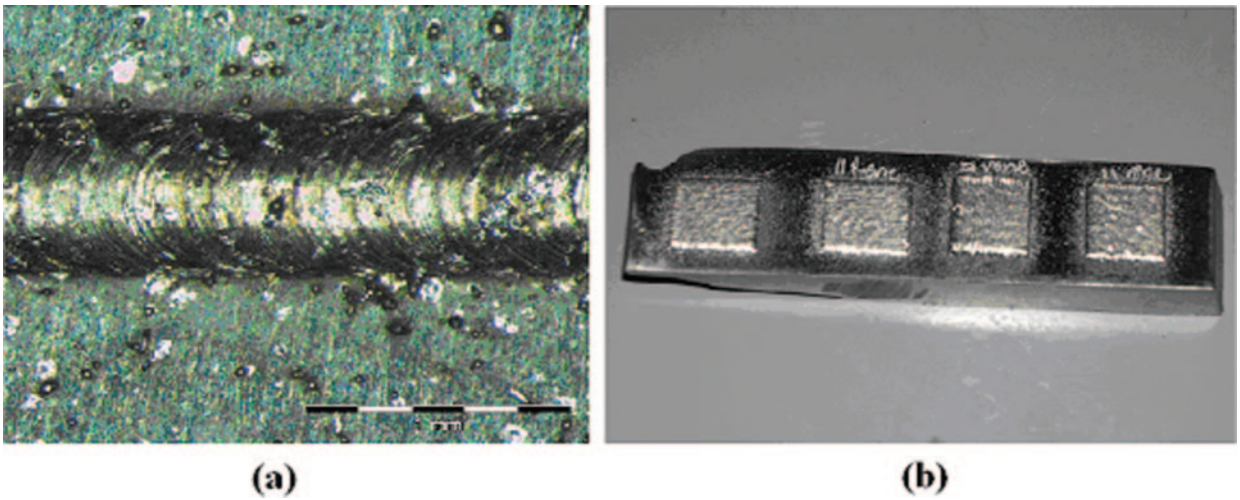

Fig. 3 (a) Single track PLPD; (b) layers of PLPD

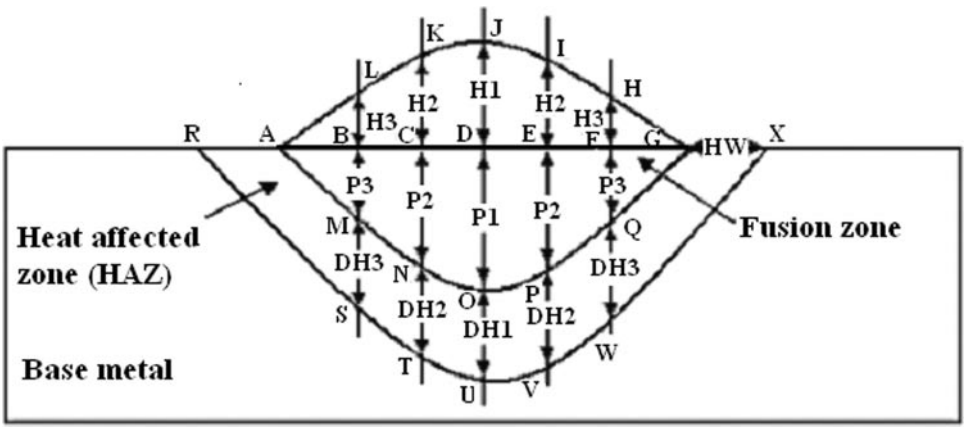

Fig. 4 Graphical mapping of PLPDs

of penetration can be appropriately represented graphically bounded by the line segments A–M. . . Q–G. . .B–A. The area of heat-affected zone (HAZ) can be similarly represented graphically bounded by the lines A–M. . .Q–G. . .G–X. . .X–W. . .S–R. . .R–A.

2.2 PLPD macrostructure preparation for graphical mapping

In the present investigation each deposit sample was cross-sectioned at two different locations and these

two cut cross-sections were polished and etched with Kalling's reagent (a mixture of 2 g $CuCl_2$, 40 ml HCl, 40 ml H_2O, and 40–80 ml ethanol (95 per cent) or methanol (95 per cent)). The macrostructures of the cross-sectioned samples were photographed and mapped as described in Fig. 4 using image analysis software [**17**]. The average of the mapped characteristics of two cut cross-sections for each sample track was used in the modelling. In all PLPD samples the HAZ could not be detected using an optical microscope. It was concluded that during the PLPD the base material is not affected severely owing to the nature of the pulsed-laser heat source, leading to non-detectable HAZ when observed through an optical microscope. The HAZ attributable to the PLPD process may be observed through a more powerful instrument, such as a scanning electron microscope. In the ANN modelling only the mapped deposition profiles of the fusion zone were used, as HAZ could not be detected in PLPD through the optical microscope.

The macrostructures of two PLPD samples with non-detectable HAZ observed through an optical microscope are presented in Fig. 5. Concave and non-concave ($P1 \leqslant P2$, Fig. 4) penetration zone shape profiles of two PLPD deposits are shown in Figs 5 (a) and (b) respectively. Some investigators have modelled the weld bead shape profile geometry by considering the top weld reinforcements to be convex and the weld penetration zones to be concave in shape [**4**, **5**]. However, from Figs 5 (a) and (b) it can be observed that the top reinforcement and penetration zone shape profiles of the PLPD deposits cannot be represented merely by convexities and concavities for every case. For the graphical representation of the PLPD deposits' shape profiles, detailed geometrical mapping is required.

3 ANN MODELLING OF PLPD DEPOSIT PROFILES BASED ON GRAPHICAL MAPPING

For the ANN modelling, the input variables used were peak pulse power, pulse duration, laser frequency, and laser traverse speed. The output layer of the ANN model representing the variables to be predicted consisted of PLPD cross-sectional area, perimeter, width (BW), heights (H1, H2, H3), and penetration depths (P1, P2, P3).

The performance of the neural network depends on the number of hidden layers and the number of neurons in the hidden layers. Therefore, many trials may be needed in choosing the optimal structure for the neural network by changing the number of hidden layers as well as the number of neurons in each of the hidden layers. The hidden and output layer neurons in a back-propagation ANN model are each connected to all of the units in the preceding layer. When the network is executed, the input variable values are placed in the input, and then the hidden and output layer units are progressively executed. Each calculates its own activation value by taking the layer and subtracting the threshold. The activation value is passed through the activation function to produce the output of the neuron. When the entire network has been executed, the outputs of the output layer act as the outputs of the entire network. There are no rules suggesting the number of hidden layers to be used in a network [**1**].

From the literature it is observed that, for better training of the ANN, two hidden layers can be conveniently used for arc welding and laser solid freeform fabrication processes [**1**, **9**, **14**, **18**]. Nagesh and Datta used two hidden layers in the back-propagation ANN model for shielded metal arc welds (SMAW) [**1**]. Toyserkani and Alimardani also used

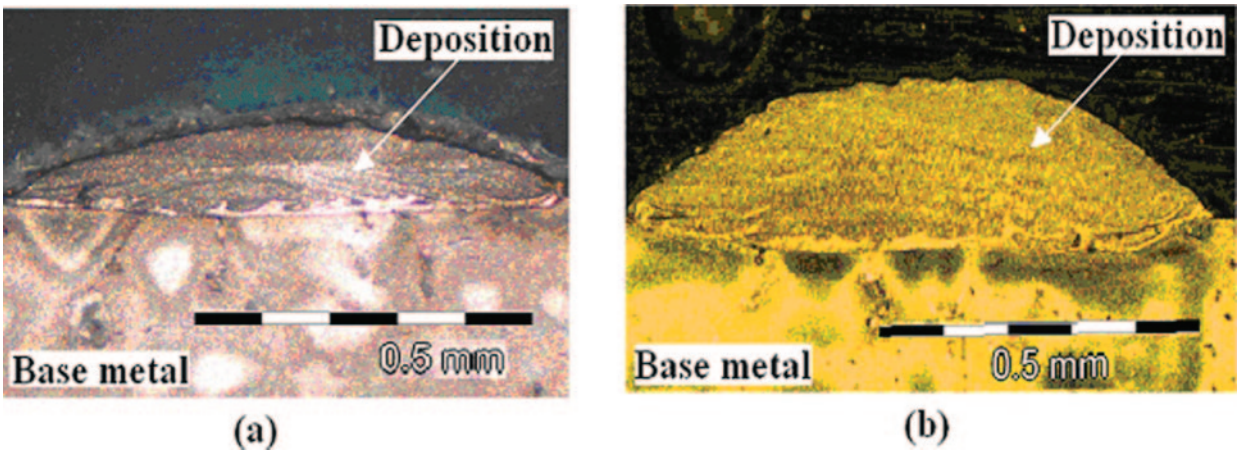

Fig. 5 Etched PLPDs with concave and non-concave penetration profile: (a) PLPD with concave penetration profile of sample no. 16, Table 2; (b) PLPD with non-concave penetration profile of sample no. 2, Table 3

two hidden layers in the ANN for modelling the laser-assisted solid freeform fabrication process [**9**]. For modelling submerged arc weldment shape profiles, an ANN model based on two hidden layers has also been used successfully [**18**]. The numbers of hidden neurons in each hidden layer were selected on a trial and error basis by these investigators [**1**, **9**, **14**, **18**].

The appropriate neural network structure for predicting single track PLPD cross-sectional area, perimeter, width, heights (H1, H2, H3), and penetration depths (P1, P2, P3) was chosen by the trial and error method [**1**, **3**, **9**, **14**, **18**]. In the current study the structure of the neural network was 4–21–21–9 (i.e. four neurons in the input layer, 21 neurons in the first hidden layer, 21 neurons in the second hidden layer, and nine neurons in the output layer). The ANN was trained with respective input process parameters (as indicated in Table 2), and outputs profile characteristics of each deposit, including each deposit profile's perimeter and cross-sectional area. The ANN inputs, outputs, and hidden layers are shown in Fig. 1. It was observed that the learning of the ANN was better when an individual deposit's perimeter and cross-sectional profile were also included in the training. The network was trained for 115 000 iterations with a learning rate of 0.5 and momentum term of 0.45. With a greater number of iterations, although the normalized system error reduced significantly, the prediction capability of the network reduced. Further training did not improve the modelling performance of the network. Kim *et al.* also used 200 000 iterations in their ANN model for predicting the weld bead geometry shape profile [**4**]. The present ANN model was verified with a number of test cases with which it had not been trained. The parameters for the test cases are given in Table 3.

4 RESULTS AND DISCUSSION

The results and discussion of the present investigation are focused only on the prediction of PLPD shape profile geometries [**4**–**5**]. The experimental data and the results of ANN modelling were not statistically interpreted to indicate the interaction effects of the process variables. The input process parameters, output profiles characteristics (H1, H2, H3, P1, P2, P3; see Fig. 4), perimeters, and cross-sectional areas of the 27 sample jobs mentioned in Table 2 were used for the training of the ANN model. During the training of the ANN the maximum error for prediction of PLPD width was found to be within 2.75 per cent. PLPD results indicated shallow penetrations in comparison with the height of deposition. The maximum PLPD height observed from the experiments was within 0.4 mm. For the trained samples the maximum error during the training for predicting the PLPD height was found to be 0.6 per cent. A similar trend was also observed for the penetration depth with maximum 0.175 per cent error during the training (Fig. 6). For each sample the penetration depths should have been at a maximum for P1 (Fig. 4) in the ideal situation. This was not observed for PLPD penetration depths. Many times P1 was found to be equal to or less than P2. The maximum penetration depth was within 0.075 mm

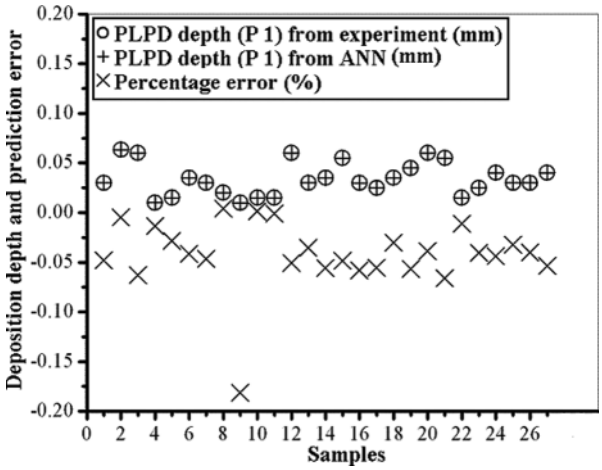

Fig. 6 Comparison of PLPD depth (P1, Fig. 4) from experiment (Table 2) and ANN model

Table 3 PLPD parameters of test samples

Test sample no.	Pulse power (kW)	Pulse duration (ms)	Laser frequency (Hz)	Laser traverse speed (mm/s)
1	3.500	2.200	4.000	0.381
2	3.500	2.800	4.000	0.381
3	3.000	2.000	7.000	0.508
4	3.000	2.800	5.000	0.508
5	3.000	2.200	7.000	0.508
6	2.500	2.000	6.000	0.381
7	2.000	2.000	4.000	0.381
8	2.000	2.800	8.000	0.804
9	2.000	2.400	8.000	0.381
10	2.000	2.600	6.000	0.381

(Fig. 6). The trained ANN model was also tested for the samples with which it was not trained. Ten samples were chosen with different pulsed-laser parameters, as shown in Table 3. The percentage of errors was slightly greater for the test cases (Table 3) when compared with the ANN results of the samples with which the network was trained (Table 2). This was due to the uncertainties associated with the PLPD process. It is not possible to have a very accurate flow of powder to the melt pool. In spite of all the precautions during PLPD, the process variance exists and it is not easily quantifiable. During the PLPD some powders may not get melted and deposited in the weld pool. The semi-melted powder particles can sometimes cling to the depositions. Some semi-melted powder particles can also be embedded in the deposit, loosely bonded, indicating a clear boundary with the deposit.

The error for PLPD width prediction from the ANN model for the test cases was found to be within 6 per cent. The mean percentage prediction errors of PLPD heights (H1, H2, and H3, Fig. 4) for the test samples (Table 3) were found to be within 8 per cent, as observed in Fig. 7. The errors for the PLPD penetration depths prediction were within 14 per cent as also indicated in Fig. 7. In most of the test cases (Table 3) for PLPD heights (H1, H2, and H3; Fig. 4) and depths (P1, P2, and P3; Fig. 4) the mean percentage error of the prediction was within 10 per cent (Fig. 7).

The test case (Table 3) PLPD deposits' shape profile geometry outputs from the ANN model were used as the inputs in the Origin graphing software for their graphical presentation. In Figs 8 to 11 the profiles of some of these test cases (Table 3) are shown. The estimated and measured top reinforcement and penetration zones of these test cases are also shown in Figs 8 to 11. The dashed lines in Figs 8 to 11 represent the estimated PLPD top reinforcements and penetration zones; the solid lines represent the measured top reinforcements and penetration zones. From these figures it can be observed that the PLPD procedure can be automated where the nature of top reinforcements, penetration zone, and entire shape profiles of the deposits can be predicted and

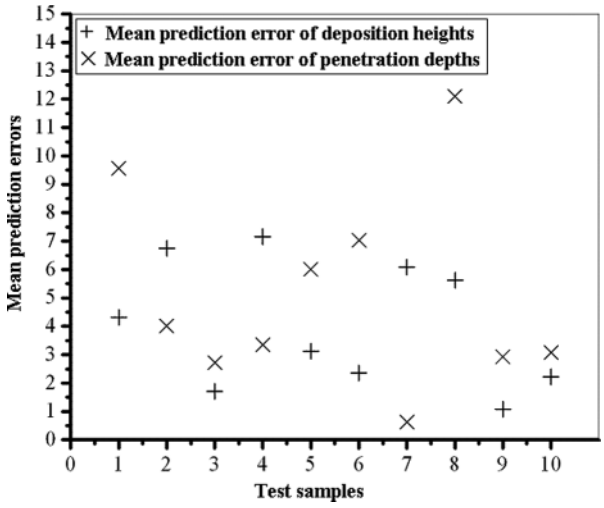

Fig. 7 Mean percentage prediction errors of PLPD heights (H1, H2, and H3; Fig. 4) and depths (P1, P2, and P3; Fig. 4) for test cases (Table 3) from the ANN model

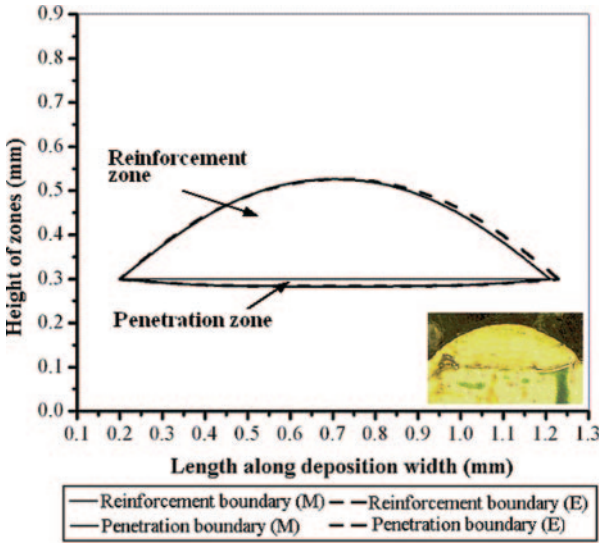

Fig. 8 Pulsed-laser powder deposition shape profiles from experiments and modelling for test case no. 1 (Table 3; E, estimated; M, measured)

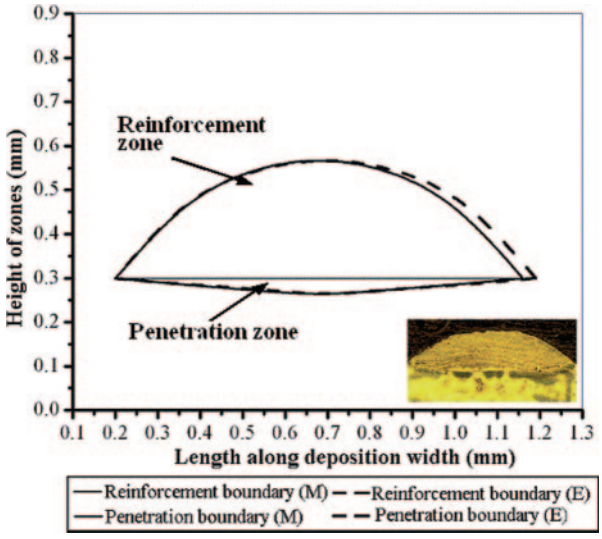

Fig. 9 Pulsed-laser powder deposition shape profiles from experiments and modelling for test case no. 2 (Table 3; E, estimated; M, measured)

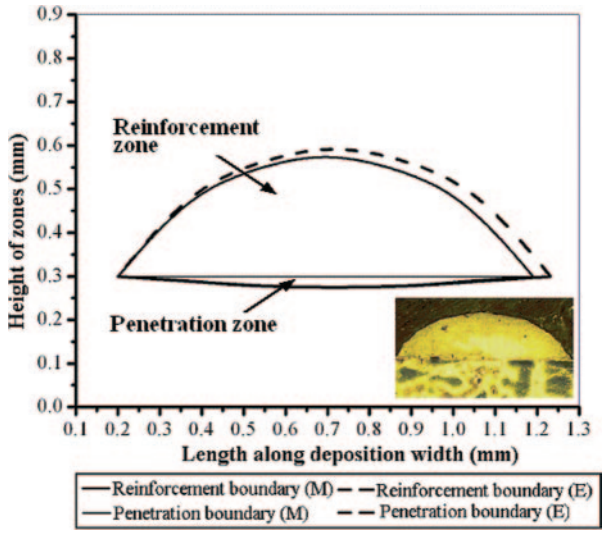

Fig. 10 Pulsed-laser powder deposition shape profiles from experiments and modelling for test case no. 4 (Table 3; E, estimated; M, measured)

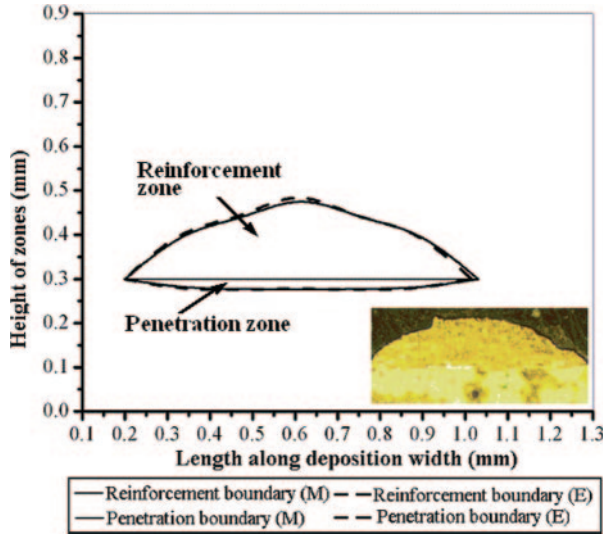

Fig. 11 Pulsed-laser powder deposition shape profiles from experiments and modelling for test case no. 8 (Table 3; E, estimated; M, measured)

graphically represented based on the pulsed-laser input process parameters.

5 CONCLUSIONS

The following conclusions related to ANN modelling of the PLPD process were drawn from the present investigation.

1. Two different PLPD cross-sectional profiles with different cross-sectional areas can have nearly the same deposit height and penetration depth. Thus a single convex index and penetration depth may not always be sufficient to represent graphically the top reinforcement and the penetration zones of a PLPD cross-sectional profile.
2. The PLPD deposit width can be divided into a number of equal segments; corresponding deposit heights and penetration depths at these segments can be used for better graphical representation of the shape profile.
3. In the present investigation a database of PLPD shape profile characteristics was developed using a detailed mapping technique and successfully used to train a back-propagation ANN. The trained ANN model developed in the present investigation was adequate for predicting the PLPD shape profile geometries.
4. The mapping technique for the deposits and the ANN modelling developed in the present investigation can be used for on-line quality control of PLPD shape profiles. An estimation of fusion zone boundaries of the deposits can also be made from the present ANN modelling of the PLPD process.

ACKNOWLEDGEMENT

The work has been partially supported by the Welding Research Council through the High Alloys Subcommittee.

REFERENCES

1 **Nagesh, S. D.** and **Datta, G. L.** Prediction of weld bead geometry and penetration in shielded metal-arc welding using artificial neural networks. *J. Mater. Processing Technol.*, 2002, **123**, 303–312.
2 **Cook, G. E., Andersen, K., Karsai, G.,** and **Ramaswamy, K.** Artificial neural networks applied to arc welding process modeling and control. *IEEE Trans. Industry*, 1990, **26**(5), 824–830.
3 **Cook, G. E., Barnett, R. J., Andersen, K.,** and **Strauss, A. M.** Weld modeling and control using artificial neural networks. *IEEE Trans. Industry*, 1995, **31**(6), 1484–1491.
4 **Kim, I. S., Son, J. S., Park, C. E., Kim, I. J.,** and **Kim, H. H.** An investigation into an intelligent system for predicting bead geometry in GMA welding process. *J. Mater. Processing Technol.*, 2005, **159**, 113–118.
5 **Kanti, M. K.** and **Rao, S. P.** Prediction of bead geometry in pulsed GMA welding using back propagation neural network. *J. Mater. Processing Technol.*, 2008, **200**, 300–305.
6 **Toyserkani, E., Khajepour, A.,** and **Corbin, S.** *Laser cladding*, 2005 (CRC Press, Boca Raton, Florida).
7 **Li, L.** Repair of directionally solidified superalloy GTD-111 by laser-engineered net shaping. *J. Mater. Sci.*, 2006, **41**, 7886–7893, DOI: 10.1007/s10853-006-0948-0.

8 **Liu, J. C.** and **Li, L. J.** Study on cross-section clad profile in coaxial single-pass cladding with a low-power laser. *Optics Laser Technol.*, 2005, **37**(6), 478–482.

9 **Toyserkani, E.** and **Alimardani, M.** Prediction of laser solid freeform fabrication using neuro-fuzzy method. *Appl. Soft Comput.*, 2008, **8**, 316–323.

10 **Vitek, J. M., David, S. A., Richey, M. W., Biffin, J., Blundell, N.** and **Page, C. J.** Weld pool shape prediction in plasma augmented laser welded steel. *Sci. Technol. Weld. Joining*, 2001, **6**(5), 305–314.

11 **Onwubolu, G. C., Davim, J. P., Oliveira, C.,** and **Cardoso, A.** Prediction of clad angle in laser cladding by powder using response surface methodology and scatter search. *Optics Laser Technol.*, 2007, **39**(6), 1130–1134.

12 **Kim, S., Son, J. S., Park, C. E., Lee, C. W.,** and **Prasad, Y. K. D. V.** A study on prediction of bead height in robotic arc welding using a neural network. *J. Mater. Processing Technol.*, 2002, **130–131**, 229–234.

13 **Jeng, J.-Y., Mau, T.,** and **Leu, S.-M.** Prediction of laser butt joint welding parameters using back propagation and learning vector quantization networks. *J. Mater. Processing Technol.*, 2000, **99**, 207–218.

14 **Mahapatra, M. M., Sadat, A., Datta, G. L.,** and **Pradhan, B.** Modeling and predicting the effects of process parameters on weldment characteristics in shielded metal arc welding. *Indian Weld. J.*, 2005, **38**(2), 22–29.

15 **HAAS-LASER GmbH.** *Laserunit HL 54P manual*, 2005, (HAAS-LASER, Schramberg).

16 **Bay State Surface Technologies, Inc.** *Model 1200 powder feeder manual*, 2003 (Bay State Surface Technologies, Massachusetts).

17 **Olympus Corporation.** *AnalySIS FIVE image analysis software manual*, 2007 (Olympus corporation, Pennsylvania).

18 **Mahapatra, M. M.** *Thermomechanical finite element analyses and experimental investigations on angular distortions and weldment characteristics of arc welded joints.* PhD Thesis, Indian Institute of Technology, Kharagpur, India, 2008.